Journal of Fluorescence
https://doi.org/10.1007/s10895-024-04027-7

RESEARCH

Profile distribution, Z-scan technique, Optical limiting and thermal lens method studies on Cyanidin-3-O-glucoside chloride

Khitam Alsaedi[1] · Abdulameer Imran[2] · Hussain A. Badran[2] · Riyadh Ch. Abul-Hail[2] · Khalid I. Ajeel[3]

Received: 25 September 2024 / Accepted: 5 November 2024

Abstract

For the purpose of determining the characteristics of the Cyanidin-3-O-glucoside chloride (COGC) dye, both an FT-IR spectrometer and a UV–Visible spect rometer were employed through the process. At a wavelength of 473 nm, a diode-pumped solid-state (DPSS) laser with an adjustable wavelength was used to quantify the thermally induced optical nonlinearity of the dye in a solvent composed of dimethylformamide. For the purpose of measuring the optical response, the Z-scan technique was utilised. The dye showed negative and large nonlinear index of refraction values, with high nonlinear absorption coefficients. The nonlinear index of refraction (n_2) and nonlinear absorption coefficient (β) of the COGC/PMMA film were measured to be $110.55\times10^{7}\ cm^2/W$ and 136.35×10^{-3} cm/W. Thermal lens technique was used to investigate thermo-optical properties and n_2. The optical limiter capabilities of the COGC dye are being investigated as a potential use.

Keywords Thermal diffusivity · Thermal lens technique · COGC dye · Optical limiting · Blooming

Introduction

Significant nonlinear optical (NOL) features have attracted a lot of attention recently and hold promise for applications in optoelectronics and photonics, including time-reversed optical wave, photonics-based computing, light wave communication, and optical limiting [1–7]. Researchers are excited about exploring organic and inorganic substances for nonlinear optical applications like optical limiting, optical switching, and optical communication thanks to their remarkable properties [8–14]. Despite their appealing NOL properties, the high cost and energy requirements of most inorganic materials limit their practical applications. To overcome the current constraints, researchers are constantly searching for new optical materials that are accessible, possess superior NOL capabilities, and respond to easily available low-power lasers. Owing to their distinct chemical characteristics, natural pigments such as flavonoids, anthocyanins, and carotenoids, are a viable and eco-friendly alternative to inorganic and synthetic materials. The exploration of novel NOL materials with sub-picosecond response times and large third-order NOL susceptibility values for photonics and optoelectronics applications remains an active research area. Recent studies using advanced techniques have demonstrated the presence of nonlinear optical properties in natural dyes extracted from flower petals, leaves, bark, seed, and other organic substances, suggesting potential applications in various fields [15–20]. Zongo et al. revealed the potential of Bixa Orellana pigments for light manipulation by demonstrating their nonlinear optical properties through a spin-coating technique [21]. Bouchouit et al. employed four-wave mixing in a degenerate system to characterize the NOL properties of carotenoids extracted from spinach leaves. A number of researchers have reported the widespread potential of various natural plants, including green wattle bark, Marigold flowers, Cocks Comb flowers [22], Curcuma longa, trigonella foenum graecum [23], egonia malabarica Lam, Melastoma malabathricum, Punica granatum L [24, 25], grape pomace [26], chlorophyll-a extracted from Andrographis paniculata leaves[27], β-carotenoid extracted from phyllanthus niruri[28], natural tomato lycopene[29], Anthocyanin extracted from blueberry[30] and blue pea flower [31], as readily accessible sources for the

✉ Hussain A. Badran
hussain_badran@yahoo.com

[1] College of Dentistry, University of Misan, Misan, Iraq

[2] Department of Physics, Education College for Pure Sciences, University of Basrah, Basrah, Iraq

[3] Department of Instrumentation Engineering Techniques, Al-Kunooze University College, Basrah, Iraq

Published online: 30 November 2024

extraction of natural dyes. Thiscontribution will confirm that the COGC dye, which is the subject of this discussion, has NOL characteristics caused by a high population of delocalized p-electrons within their anthocyanin squeleton. This leads to a large generation of third harmonics and the phenomena of two-photon absorption, such as the attractive intensity-dependent refractive index and optical limiting. This research used a Fourier transform infrared spectrometer and a UV–visible spectrometer to characterize a natural dye compound containing the anthocyanin group (Cyanidin-3-O-glucoside chloride (COGC)). The n_2 and the β of the COGC dye were studied with a diode-pumped solid-state (DPSS) laser with an output power of 18 mW at 473 m using the Z-scan technique, based on the sample-induced changes in a beam profile at the far field. The study was conducted on different concentrations of the COGC dye and COGC/PMMA film. The optical limiting effect was also studied. The application of Thermal lens technique to study the thermo-optical properties and nonlinear index of refraction properties of anthocyanins groups is here discussed elaborately.

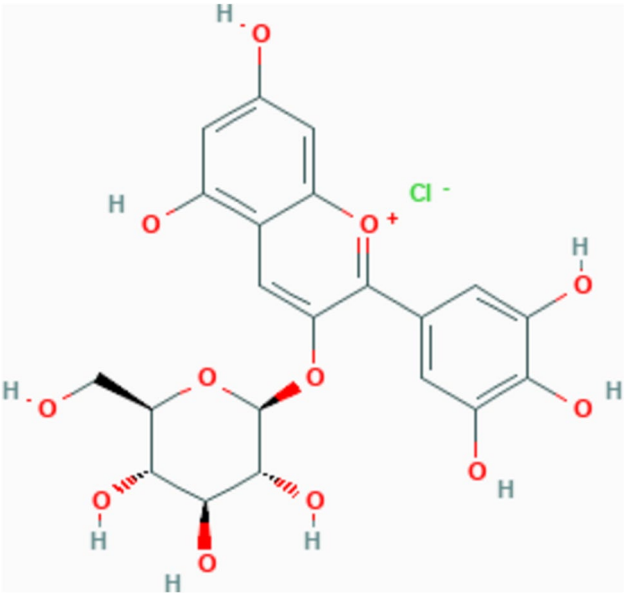

Fig. 1 Structure of COGC dye

Experimental Procedures

Sample Preparation

In the present study, we use two types of materials: We have selected Cyanidin-3-O-glucoside chloride purchased from AdooQ Bioscience company, which has a molecular formula of $C_{21}H_{21}ClO_{12}$ and a molecular weight of 484.83 g/mol, for the present experiment. The second material is dimethylformamide (DMF) solvent which was supplied by Sigma-Aldrich, which was of 99% purity. Figure 1 illustrates the chemical arrangement of the Cyanidin-3-O-glucoside chloride dye. The sample was prepared as follows: We separately dissolved 0.0436 g of Cyanidin-3-O-glucoside chloride dye in DMF solvent. We used medium-fast paper filters, measuring 0.33 mm in thickness and 55 g/m^2 in weight, for filtration and used a hot plate magnetic stirrer for 2 h to create a consistent solution. The yield concentration is set at 0.5 mM. We prepared the other samples for the DMF solution of COGC in a similar manner, with 0.1 and 0.3 mM concentrations.

During the process of preparing the solid films, we decided to use poly-methyl methacrylate (PMMA) as the host material for the production of dye-doped polymer film. We obtained this material from Aldrich, which was of 99% purity. The DMF solvent was used to dissolve 0.133 gm of the COGC dye. The concentration of the solvent was 10 mM. After stirring the solution that was produced at room temperature for forty-five minutes, we filtered it through a 0.2 μm syringe filter in order to get a concentration of nine millimoles. In the event that we were interested in determining the weight of the substance that we needed to melt to fulfil the requirement, we calculated [32]:

$$M_{mc} = \frac{W_w}{M_{mt}} \times \frac{1000}{V_{solv}} \tag{1}$$

Here, M_{mc} is the molar concentration (Mol/L), W_w represents the total amount of dye dissolved in the solution (gm), M_{mt} is the Molecular weight (gm/mol) and V_{solv} is the volume of DMF (ml). 3gm of PMMA polymer dissolves in 35 ml of DMF solvent. Using the relation [33, 34]:

$$C_{con} = \frac{W_{pw}}{V_{DMF}} \tag{2}$$

Here, C_{con} denotes the polymer concentration, W_{pw} is the weight of PMMA, V_{DMF} is the volume of DMF solvent. COGC film was prepared by the casting method. We combined the COGC solution with PMMA at a volume ratio of 1:1 to achieve the desired result. In order to guarantee that the components were well combined, the COGC /PMMA combination was mixed for a period of fifteen minutes. Using a mechanical pipette, a portion of the homogeneous solution was extracted, and then it was put onto a clean glass slide. The substrate was then kept in the laboratory for forty-eight hours in order to get a homogenous polymeric layer. The thickness of the films was around 5 µm.

Morphology of COGC Film

Film Rroughness

In order to investigate the surface topography of an COGC /PMMA film, atomic force microscopy (AFM) were utilised. Additionally, atomic force microscopy was utilised in order to conduct a roughness study. Homogeneity and the absence of flaws were observed in the film, which had dark micrometre regions that corresponded to COGC dye molecules and brilliant micrometre regions that were assigned to PMMA chains [35]. Figure 2a and b compressed structures and an equitable distribution of dye particles inside the polymer matrix were seen in the three-dimensional and two-dimensional AFM pictures. The values of the roughness parameter for the film were as follows: The Arithmetic mean absolute height (R_a) for the COGC /PMMA film is 9.333 nm, and the Skewness (R_{sk}) is 0.527 nm. Kurtosis (R_{ku}) is a crucial parameter used to determine the homogenous of a surface, whether it is a rough surface ($R_{ku} < 3$) or a spiky surface ($R_{ku} > 3$). The R_{ku} values for the COGC /PMMA film were 2.137 nm, confirming that the film has a rough surface. Additionally, the root means square roughness (R_q) of the COGC / PMMA film is 13.22 nm. The performance of materials in a variety of applications, such as electrical audio devices, sencer, electroacoustic, and biomedical devices, may be evaluated with the assistance of these approaches because to their versatility [36–39].

Profile Distribution

Surface roughness increases both diffusion and transmission, so high-precision measuring devices must have a characterized surface topography. Among the most important applications of roughness features in linear and nonlinear optics are the linear electro-optical effect, optical filters, and optical storage systems. The method of image processing enables the characterization of surface morphology by imitating optical operations for the purpose of measuring surface roughness. Two common morphological features are shown by the surface profile distribution of the PMMA film. These characteristics include evenly scattered granular characteristics on various scales,

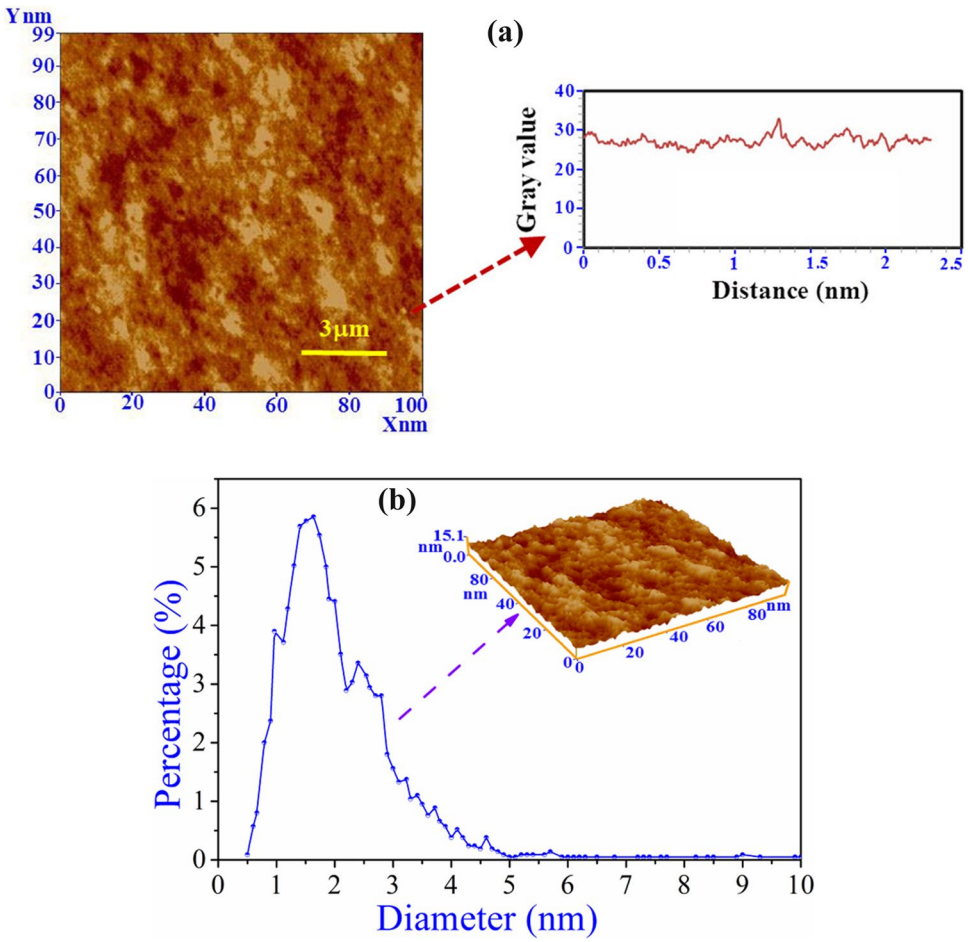

Fig. 2 (a) 2D, (b) 3D ATM images and Gray distribution of COGC/PMMA film

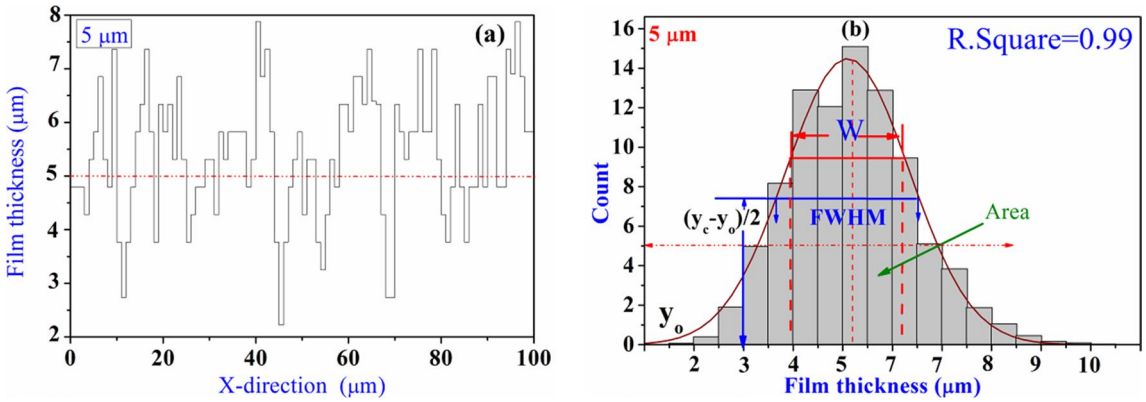

Fig. 3 Shows the morphology study of the COGC /PMMA film. (a) Surface morphology scan along the film's region. (b) Homogeneous Gaussian thickness distribution

with uneven shapes, sizes, and separations among them. Through a visual analysis of Fig. 3-a and b, these traits may be clearly detected.

As a result, we utilised the scan along the region of the PMMA film in order to establish that the distribution was comparable throughout. On the other hand, it demonstrates that the sample follows a Gaussian distribution that is homogenous. Furthermore, the distribution demonstrates that the area under the curve is homogeneous, with a width of 2 μm (W = 2 μm) and a curved distribution equal to $y_c = y_0 + A/(W * Sqrt(\pi/2))$. To our knowledge, the sample did not exhibit any signs of aggregation. A He–Ne laser beam with a power of 4 milliwatts travels across the film to test its optical quality. For this research, we acquire film that does not display any distortion or dispersion of the laser beam.

FT-IR Analysis

Spectroscopy measurement via an FT-IR device. The sample shown in Fig. 4 were tested using an FT-IR device, specifically a Vertex 70 from a broker company. The sample spectra were reported as a distribution of the samples by (ir) disc in potassium bromide (KBr) for a 1 mgramme experiment with 200 milligrammes of KBr within a wavelength range of 400 to 4000 cm^{-1} and a scan size of 1 cm^{-1}. Functional groups in a sample can be identified by FT-IR spectroscopy analysis by matching absorption peaks to the vibrational modes of chemical bonds (see Fig. 4). The broad absorption band observed at 3326 cm^{-1} is characteristic of O–H stretching vibrations in hydroxy groups. Two absorption bands observed at 2936 cm^{-1} and 2890 cm^{-1} confirm the presence of a methylene group in the sample. The relative intensity ratio of these peaks corresponds to the symmetric and antisymmetric stretching modes of C-H bonds in a methylene group, respectively. The higher wavenumber

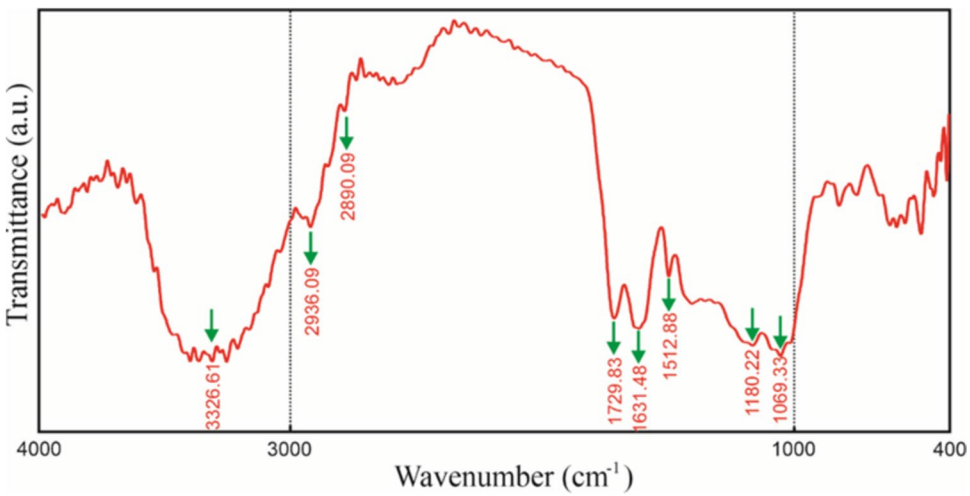

Fig. 4 The FT-IR spectroscopy of COGC dye

(2936 cm^{-1}) is attributed to the symmetric stretch due to the identical movement of both C-H bonds.

Furthermore, the spectrum exhibits a strong peak at 1729 cm^{-1}, characteristic of the C = O stretching vibration in a ketone group. Additionally, the spectrum reveals characteristic peaks at 1631 cm^{-1}, 1180 cm^{-1}, and 1069 cm^{-1}, corresponding to aromatic C = C stretching, C-O stretching in an ether group, and C-O stretching in an alkoxy group, respectively. The stretching vibrations found in the pigment of Alcea rosea and observed in the IR spectra have indicated the existence of chemical groups associated with the anthocyanin group.

UV–Vis Absorption Investigations

The absorption of the incident light leads to an electron transfer to the required energy states, which determines the linear light transmission response of the substance. This process makes the electronic band structure determinable and allows for the trajectory of electrons to distinct energy states [40, 41]. UV–Vis absorption spectra were acquired in the 200–600 nm range using a GBC Cintra 2020 UV–Vis spectrometer. The UV–Vis absorbance spectra of the samples at different concentrations are presented in Fig. 5. The maximum absorption wavelength of all samples remained relatively constant around 509 nm, regardless of concentration. However, the peak intensity exhibited a significant increase with increasing concentration. The absorption spectra observed in Fig. 5 confirm the $\pi \rightarrow \pi^*$ transition occurring within the conjugated system within the chromophore (light-absorbing group) of the COGC dye molecule.

The estimated energy gaps of polymer film is 2.6 eV while the obtained values of energy gaps were 1.84, 1.72 and 1.63 eV for concentration of 0.1 mM, 0.3 mM and 0.5 mM respectively. In most cases, there are gaps between the particles in a liquid, yet they are still in contact with one another. A liquid's structure is incredibly erratic. While orbitals on distinct atoms frequently have mismatches in energy or overlap, on rare occasions they coincide and mix, leading to a great deal of local mixing. It appears that solids and liquids have somewhat distinct electrical structures for quite different reasons. Because homogeneous and inhomogeneous broadening have distinct sources, the origins of bands non liquids and solids vary. Both scenarios result in bands (an energy distribution); however, the first scenario involves broadening over resonantly matched orbitals on distinct atoms or molecules, while the second scenario involves changes in the local environment as a result of randomly fluctuating perturbations brought on by nearby molecules (referred to as "the solvent"). In the first example, homogenous broadening is caused by Pauli's exclusion principle and excessive orbital mixing. In the case of a liquid, motional jostling causes inhomogeneous widening. The energy in a liquid can be changed by bonding, but it can also be disturbed by molecules with different orbitals. As a result, we calculated the energy gaps in Fig. 5 using the average of the gaps that don't change depending on the concentration.

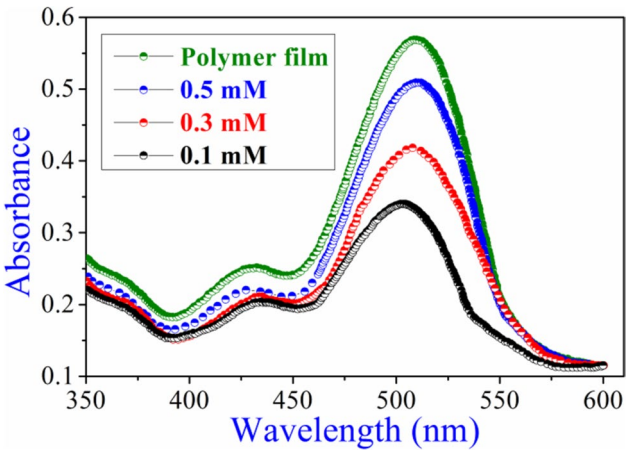

Fig. 5 UV–Vis profile of COGC dye solution and polymer film

Z-scan Configuration

The use of the Z-scan method has become widely adopted for studying optical nonlinearities in various optical materials because of its sensitivity and ease of use. In this approach, the sample is translated along the longitudinal axis of a focused Gaussian beam, and the intensity of the far-field is recorded as the sample position changes. However, even when maintaining a constant input power, the sample meets varied incident fields at different Z-positions.

Z-scan refers to the spatial and temporal characteristics of the input beam as it travels through the sample during the experiment are important, causing significant distortions. Figure 6 presents the experimental setup for the z-scan approach. We conducted the experiment using an adjustable diode-pumped DPSS laser. The laser output power can be varied over the range of 0–100 mW emitting a Gaussian beam at 473 nm with a power of 18 mW was used for the stimulation. The laser Gaussian beam was focused to

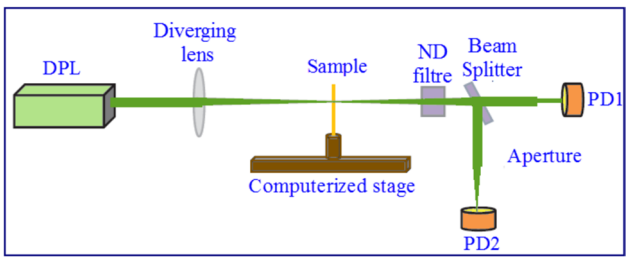

Fig. 6 Schematic diagram of the Z-scan setup

a beam waist ($\omega_\circ$) of 22.19 µm by a positive lens of focal length + 5 cm and passed through the sample, either a 0.1 cm quartz cell containing COGC dye solution or COGC: PMMA film. In this research, the experiment was carried out by moving the sample in the direction of the z-axis while it was being moved across the focal length point. During the closed-aperture z-scan (CAZS), the transmitted power output was measured using an aperture with a tiny diameter that was located in the far field of the lens. This measurement was performed as a function of position z of the COGC concerning the focal plane (z = 0). The measurement was made using a digital power meter and the photo-detector PD_2. In addition, the photo-detector PD_1 is connected to a digital power meter, which was utilized to measure the laser power that was input. In the open-aperture z-scan (OAZS), the aperture is completely open (S = 1), and the photo-detector PD_2 was used to determine the strength of the whole laser beam that was delivered through the sample.

Results and Discussion

Nonlinear Optical Properties Study

Z-scan configuration was employed to investigate the optical nonlinearity of COGC /PMMA film and solutions at three different concentrations. The closed and open aperture configurations were used, with an input beam intensity of 2.327 kW/cm^2. The sample position (z) relative to the focal point (z = 0) varies light intensities due to the spatial intensity profile of the beam. The effect of both saturable and reverse saturable absorption processes is the predominant contribution to the nonlinear absorption coefficients, β, of materials. Saturable absorption causes an intensity-dependent decrease in absorption, whereas reverse saturable absorption leads to the opposite behavior. The spectral response of sample is described by [39–41]:

$$\alpha(I) = \frac{\alpha_\circ}{1 + \frac{I}{I_s}} \tag{3}$$

The irradiance rises as the sample gets closer to the focus, and as a result of nonlinear optical absorption, the transmittance falls. Since the irradiance is strongest in the focus, nonlinear optical absorption reaches its maximum there.

$$n(I) = n_\circ + n_2 I \tag{4}$$

where $n(I)$ is the overall refractive index of the material. Alternatively, Eq. 4 may be written as [42–45]:

$$n(I) = n_\circ + \Delta n \text{and } \Delta n = n_2 I \tag{5}$$

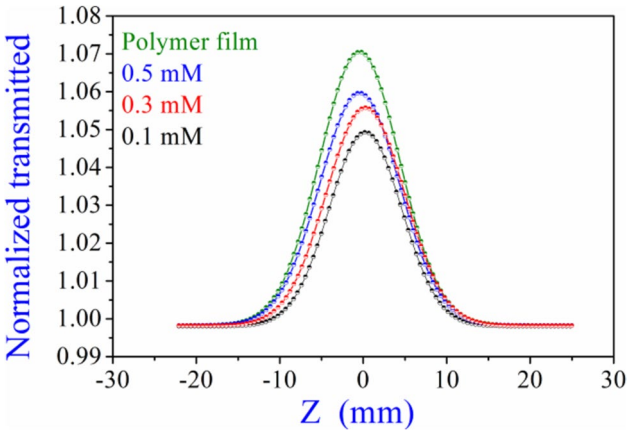

Fig. 7 Open aperture Z-scan curve

Here, $\alpha_\circ$ represents the inherent material property of linear absorption, I_s captures the material-dependent saturation intensity, and $n_\circ$ and n_2 denote the linear and nonlinear index of refraction of the sample, respectively. Figure 7 presents the OAZS of the COGC dye at an input intensity of 2.327 KW/cm^2. A concentration-dependent increase in peak transmittance is observed in the Z-scan curves, with higher concentrations showing a significant rise compared to lower concentrations (see Fig. 7). This trend suggests saturable absorption (SA) behavior. Saturable absorption is a nonlinear optical phenomenon that manifests at high input intensities. As excited state populations relax back to the lowest energy state, the substance regains its ability to absorb photons. The process of electrons dropping is significantly faster than their stimulation when low-intensity light rays directed at a material medium generate a zero population shift between the excited levels and the ground level. The high-intensity photons from the incident rays activate and move the electrons to the excited energy level. There are few electrons at ground level when the incident pulse duration is significantly shorter than the electron fall time. The material medium does not absorb as much of the incident rays as it did in the case of low-intensity light when the cross-section of photon absorption at the stimulated level is less than the cross-section of photon absorption at the ground level. We refer to this procedure as saturation absorption. For many materials, the absorption coefficient falls with high laser beam intensities. The normalized transmittance (ΔT) obtained from the OAZS measurement in Fig. 7 allows for the determination the values of nonlinear absorption coefficients β, using the relation [46, 47]:

$$\beta = \frac{2\sqrt{2}\Delta T_{ope}}{I_\circ L_{effec}} \tag{6}$$

In Eq. 6, ΔT_{ope} signifies a single peak transmittance point within the OAZS curve [48, 49], and I_o is the input laser beam intensity at the focal point, calculated as $2P_{pow}/\pi\omega_\circ^2$ [50, 51], where P_{pow} is the laser beam power and ω_o denotes the beam radius at the focus. The term L_{effc} represents the effective interaction length of the sample, which is calculated as [52, 53]:

$$L_{effc} = \frac{1 - \exp\left(-\alpha_{abso} D_{thic}\right)}{\alpha_{abso}} \tag{7}$$

D_{thic} represents the physical thickness of the sample, and α_{abso} is the material's optical linear absorption coefficient.

The Z-scan curves in Fig. 8, representing the nonlinear refraction behavior for COGC:PMMA film and solutions samples, all exhibit a peak followed by a valley in the transmittance profile. This observation ensures a negative nonlinear index of refraction ($n_2 < 0$) for the material (self-defocusing). The equation describing the normalized transmitted obtained from the pure close-aperture Z-scan measurement, as represented by the Z-scan data in Fig. 8, is given by [54, 55]:

$$\Delta T_{P-V} = 0.406\left(1 - S_{Tran}\right)^{0.25} \Delta\Theta \tag{8}$$

where ΔT_{P-V} is peak and valley transmittance, S_{Tran} representing the aperture linear transmittance is given by [56]:

$$S_{Tran} = \exp\left(1 - \frac{r_\alpha^2}{\omega_\alpha^2}\right) \tag{9}$$

The quantities r_a and ω_a are the radius of the aperture and the radius of the beam at the aperture, respectively. The term $\Delta\Theta$ represents the on-axis phase shift. nonlinear index of refraction, n_2, of the sample is described by the following relation [57, 58]:

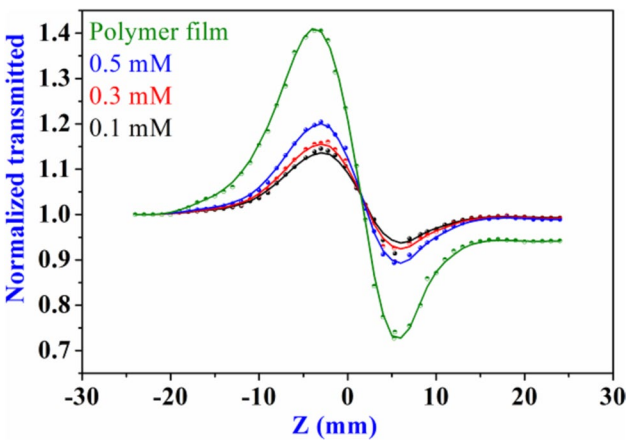

Fig. 8 Close aperture Z-scan curve

$$n_2 = \frac{\Delta\Theta}{I_\circ k L_{effec}} \tag{10}$$

where k represents the wavenumber of the light. The remarkable self-defocusing process in the COGC dye solution and COGC /PMMA film is likely attributed to thermally induced nonlinearity arising from the continuous-wave laser light at 473 nm wavelength. This indicates that the absorption of laser light leads to a temperature increase within the sample, which consequently influences its refractive index and induces a negative nonlinearity. The propagation of a Gaussian laser light within an attenuating medium induces a spatially non-uniform temperature distribution due to localized energy deposition. This variation in temperature leads to a corresponding spatial modulation of the refractive index within the material [59]. The nonlinear refractive response of the sample can arise from various mechanisms, including molecular reorientation, electrostriction, electronic nonlinearity, or thermal effects [60]. The nonlinear optical response of several materials, including semiconductors, polymers, metal nanoparticles, dyes, and liquid crystals, can be effectively enhanced by photothermal effects. The primary cause of the medium's nonlinear optical response is the absorption of incoming light by materials and its subsequent conversion to heat as a result of photothermal processes. When photons are absorbed by the substance, electromagnetic energy is transformed into thermal energy. By increasing the local temperature of the medium, this technique modifies its refractive index and other optical characteristics. When a laser beam is closely concentrated and some of its energy is locally absorbed by a substance, thermal nonlinearity results. This means that electromagnetic energy is absorbed and transformed into heat, raising the temperature of the medium locally. Because the refractive index plays a crucial role in nonlinear optical processes, this results in a change in the material's refractive index due to the heat impact (the Kerr effect phenomenon is initiated across the medium). Because the refractive index fluctuates with temperature, the material's optical characteristics alter and can lead to phenomena like thermal lensing and self-focusing. In high-intensity laser applications, where the local heating impact can cause large changes in the material's optical behaviour, this thermal nonlinearity is particularly essential.

The peak-valley distance in a Z-scan experiment (closed-aperture) is not necessarily larger in one configuration compared to the other. However, a larger peak-valley separation can enhance the sensitivity for measuring the real part of nonlinear index of refraction and minimize the influence of linear absorption [61]. The calculated nonlinear optical parameters of the COGC /PMMA film and dye solutions are listed in Table 1. The values for nonlinear refractive index (n_2) and nonlinear coefficient of absorption (β) of present samples under CW laser excitation obtained in this study are

Table 1 Calculated NOL parameters of COGC dye

Sample	$n_2 \times 10^{-7}$ (cm^2/W)	$\beta \times 10^{-3}$ (cm/W)	$\Delta n \times 10^{-4}$	ΔT_{ope}	$\Delta\Theta$
0.1 mM	0.27	0.773	0.62	0.049	0.64
0.3 mM	0.31	0.893	0.72	0.054	0.72
0.5 mM	0.44	0.98	1.03	0.058	0.98
Polymer film	110.55	136.35	257.3	0.07	2.13

in the same order (10^{-7} and 10^{-3}) with the values reported for natural carotenoids [62], novel organic compound (E)-N-(3-(3 (4(dimethylamino) phenyl) acryloyl) phenyl) quinolone-2-carboxamide [63], Silicon Carbide Doped PVA Nanocomposites [64], isoniazid-vanillin hybrid [65] and Schiff base (E)-N'-(4-(dimethylamino) benzylidene) isonicotinohydrazide[66]. Because of the various processes that are involved, the values that are provided in Table 1 with a continuous-wave (CW) laser have not been compared with the value that has been reported with pulsed lasers. Considering these findings, it appears that the cyanidin-3-O-glucoside chloride may have prospective uses in the field of nonlinear optics.

Optical Limiting Effect

The growing trends in lasers in optoelectronics and photonics necessitate stringent safety measures to preserve critical components and eye health from elevated light intensity. The emergence of adjustable and multi-spectral lasers emitting across the entire visible spectrum has rendered passive spectral filters inadequate for comprehensive eye protection from laser radiation. Advanced materials or devices are crucial for protecting optical components and human eyes from all laser wavelengths, particularly against nonlinear effects. Nonlinear optical materials-based optical power limiters offer a promising solution in this regard. These devices hold significant potential for applications in optical sensors and eye protection, leveraging nonlinear refraction (self-defocusing) as their operating principle. Optical limiters act as intensity-dependent filters, transmitting low-intensity light while significantly reducing the intensity of high-power beams [67, 68]. The optical limiting effect of the polymer film and dye solution with different concentrations was studied by using a 100 mW CW-DPSS laser at 473 nm, as shown in Fig. 9. In this configuration of the optical limit, the laser beam was focus by a lens with focal length + 5 cm. The sample is kept at the position away from focus and propagated through a sample (dye concentration or COGC:PMMA film). A variable-diameter aperture is placed to control the beam profile of the laser transmitting the sample cuvette. The photodetector (Field Max II-To + OP-2 Vis Senser) attached to the power meter measures the matching output intensity values when the input laser intensity is changed methodically.

The optical limiting behavior is depicted in Fig. 10-a for polymer sample and dye solutions. As shown in Figure for each sample, the output power exhibits linear dependence on the applied power at low input values, with the linear transmittance adhering to Beer-Lambert's law. However, as the input power increases beyond this low-power regime, the transmittance deviates from linearity, marking the saturation of optical limiting behavior. Figure 10-b illustrates the optical clamping threshold or the point at which a high-intensity light beam saturates the gain in a laser medium. Once the laser reaches this threshold, additional input power does not lead to an increase in the output power, It can be seen from the Figure that the saturated output value decreases with an increasing concentration. Optical clamping threshold of the dye solutions are 6.6, 6.6 and 6.4 mW, respectively. The pattern seen in Fig. 11 makes it abundantly evident that the optical limiting behaviour of the COGC is caused by reverse saturable absorption. In the case of the COGC solutions or the polymer film, it is important to take note of the fact that the observed optical limitation is comparable to that of synthetic long conjugated organics with various p-electron conjugation bridge architectures, as reported by Guang et al. [69].

The normalized transmission curve for 0.1 mM, 0.3 mM, and 0.5 mM solutions, as well as polymer film, are depicted in Fig. 11. This curve relate to the sample concentration. In terms of quantitative differences, the optical limiting capabilities are distinct. We have determined that the optical

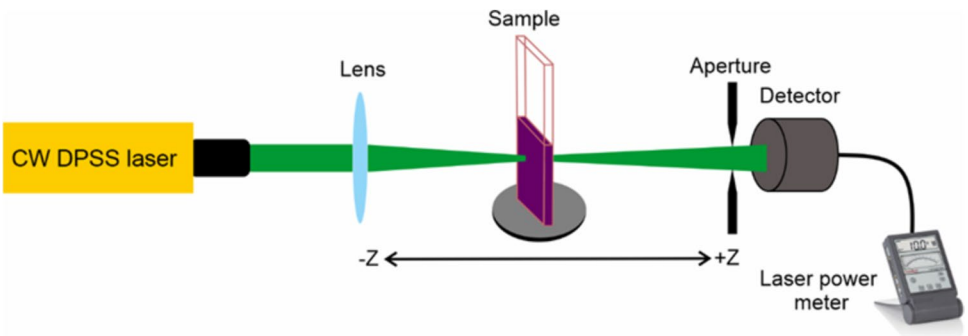

Fig. 9 Optical limiting setup configuration

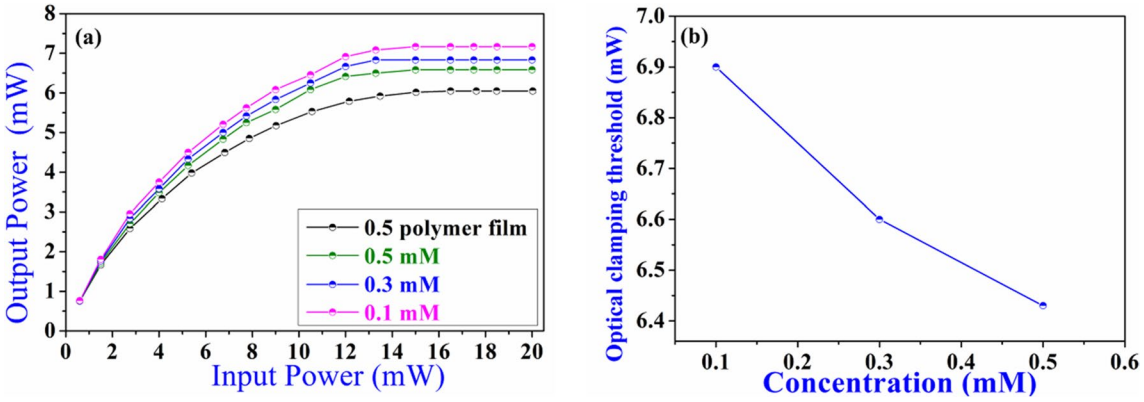

Fig. 10 (a) Optical limiting mechanism, (b) Concentration dependence of optical clamping threshold value of sample for a dye solution

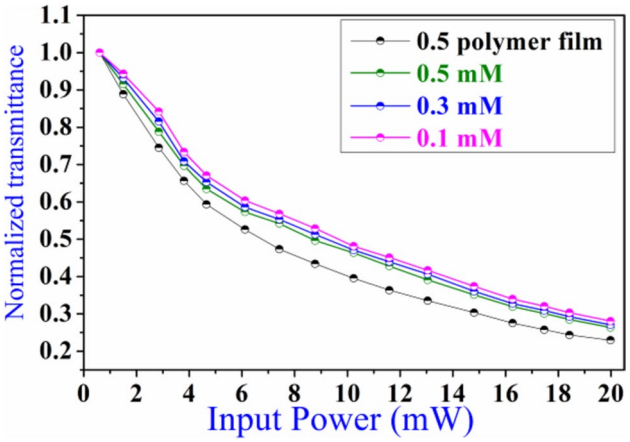

Fig. 11 Limiting thresholds data

limiting thresholds, which are defined as the incident input power at which the transmission decreases by fifty percent, are 9.6, 9.1, 8.6, and 6.7 mW, respectively, after conducting the necessary measurements. When it comes to optical limiters, materials that have lower values of limiting threshold, are typically thought to be more effective.

The fact that the various concentrations play a very significant part in the optical limiting action is something that is quite well recognized. As the dye concentration increases, this leads to a decrease in transmittance and an increase in the optical limiting effect [70]. Therefore, the optical limiting responses of the sample with a low concentration are often significantly less than those of the sample with a high dye concentration. On the other hand, the sample with a high concentration demonstrates substantial optical limits within the scope of this research. Nevertheless, to successfully investigate optical limiting, it is critical to carefully select the sample concentration in order to approach the threshold. All of the samples exhibit limiting behavior primarily due to nonlinear refraction. The nonlinearities that have arisen are mostly thermal. This is because the samples were pumped with a continuous-wave laser beam.

Thermal Lens

Two TEM_{oo} Gaussian laser beams were utilised in the dual-beam mode-mismatched Thermal lens (THLS) approach to illuminate the sample. One beam was used to excite the sample, resulting in a local temperature increase that created a lens-like element in the heated region, while the second beam was used to investigate the thermal effect. Measuring the beam centre intensity in the far field allows one to monitor the temporal change in the optical path length of the probing beam as it passes through the constructed lens. This approach creates a temperature gradient in the sample by focusing the laser beam through a lens, and this creates a spatial gradient in the refractive index [71, 72]. As the nonlinear material in the experiment, the 0.5 mM Cyanidin-3-O-glucoside chloride dye sample was created in a glass cell with a thickness of 0.1 cm. The device is made up of a single transistor logic modulated laser beam with a diode laser 6 mW output and a beam radius of 1.5 mm at a wavelength of 473 nm. It also includes a positive glass lens with a focal length of + 50 mm, a quartz cell that is 0.1 cm thick and filled with a sample of 0.5 mM, Two power instruments are required to quantify the input and transmitted output beam powers as they pass through the cell, a Lodestar oscilloscope model MOS-620CH, and a frequency generator model EM1634. The laser's output is varied at a frequency of 20 Hz in order to evaluate thermal lens (thermal blooming (THBO)). Figure 12 depicts the experimental configuration.

The fundamental method for measuring TEBO, as shown in Fig. 12, involves utilising a laser beam with the proper frequency that is focussed using a long focal length lens and then allowed to grow. One Rayleigh length beyond the focal plane is where the sample is situated. Remember that the depth of focus is determined by the Rayleigh length, $Z_{RL} = 3.2mm$. In the

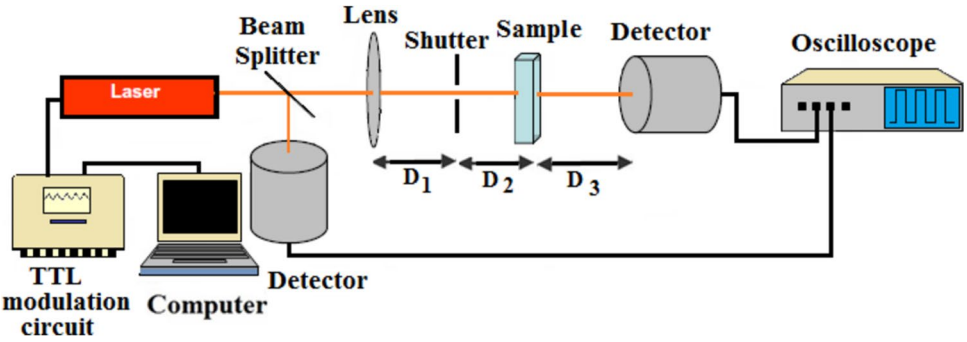

Fig. 12 THBO experimental setup

case of a TEM_{oo}, it is proportional to $\exp\left(-2r^2/\omega_\circ^2\right)$, where r is the radial distance from the beam's axis. This can be found using the formula $Z_{RL} = r\omega_\circ^2/\lambda$ [73]. The heat produced in the absorption zone raises the local temperature, which changes the refractive index and creates an optical lens. Depending on the sign of $\partial n = \partial T$, the temperature coefficient of the medium's refractive index, the optical lens may be converging or diverging. It is a negative lens for most liquids, meaning they spread when heated [74]. We take a measurement by rapidly opening a shutter on the focal plane. The THLS develops over a few tenths of a second. The laser beam appears as a point on a plane a few meters beyond the sample during that period. The spot "blooms" or grows in size. It is not required to quantify the size of the spot; a small photodiode detector placed carefully in the centre of the spot generates a photocurrent that is proportional to the laser intensity on axis and hence inversely proportional to the beam area. As the region blooms, the photocurrent decreases, according to the expression [75].

$$\frac{I(x,t)-I(x,t=\infty)}{I(x,t=\infty)} = \frac{\left[1-\frac{\theta}{2}\tan^{-1}\left[\frac{2x}{3+x^2+(9+x^2)(t_c/2t)}\right]\right]^2}{\left[1-\frac{\theta}{2}\tan^{-1}\left[\frac{2x}{3+x^2}\right]\right]^2} - 1 \tag{11}$$

$I(x,t)$ represents the intensity that is recorded in the centre of the beam, $I(x,t=\infty)$ represents the intensity that is measured at the detector after a sufficient amount of time has passed such that a steady state temperature difference is reached $x = z/z_R$ and

$$\theta = \frac{P_{pow}\alpha_{abso}L_{effec}}{\lambda K}\frac{dn}{dT} \tag{12}$$

where z is the distance between the sample and the waist of the beam, The thermooptic coefficient is denoted by dn/dT, while the thermal conductivity variable is denoted by K_{th}. The usual thermal time of the medium, denoted by the letter t_c, may be stated as[76]:

$$t_c = \frac{\omega_\circ^2}{4D_{diff}} \tag{13}$$

D_{diff} is the thermal diffusivity may be expressed as [77]:

$$D_{diff} = K_{th}/\rho_{dens}C_{sp} \tag{14}$$

ρ_{dens} is the sample density and C_{Sp} is the specific heat of the sample.

For the thermal nonlinearity and steady state case, the on-axis change in the refractive index,Δn, can be expressed as [78]:

$$\Delta n = \frac{dn}{dT}.\frac{I\alpha_{abso}\omega_\circ^2}{4K_{th}} \tag{15}$$

The transient signals of a Cyanidin-3-O-glucoside chloride dye in DMF is shown in Fig. 13 for a pumping power of 18 mW. The solid line corresponds to the data fitting of Eq. 11 to the THLS experimental data, leaving θ and t_c as adjustable parameters. Using the value of $\alpha_{abso} = 7.1623cm^{-1}$, t_c from the fit and keeping in mind that $\theta = -(P_{pow}\alpha_{abso}L_{effec}/\lambda K_{th})\Theta(dn/dT)$ (Eq. 12), $n_2 = (-3.799\times10^{-7}\ cm^2/W)$ was obtained when $K_{th} = 0.185\ Wm^{-1}K^{-1}$ and Θ (the fraction of absorbed energy) is converted into heat per photon. In the case of COGC non-luminescent dye, such as the dye studied in this paper, all the absorbed energy is converted into heat [79, 80], so that$\Theta = 1$. The value of the enhancement factor, $E = (-dn/dT)/(1.91\lambda k)$, was calculated for 5 mW power [42] to be 380.30 W^{-1}. The computation values fort_c,θ,D_{diff} and dn/dT are given in Table 2.The standard error of the estimated optical properties was $\pm 2.833\%$. Table 2 presents the THLS data,t_c,θ, D_{diff} and dn/dT of several samples and our finding. Where, the Cyanidin-3-O-glucoside chloride sample shows good agreement with the other materials. The thermal lens signal is dependent on two factors that vary with temperature, namely dn/dT and K_{th}, the other factors of Eq. 12 remaining constant.

Conclusion

Cyanidin-3-O-glucoside chloride dye was generated in two distinct forms: as a solution with varying concentrations and as a thin film by doping PMMA material. The thin film was then coated onto glass substrates using the

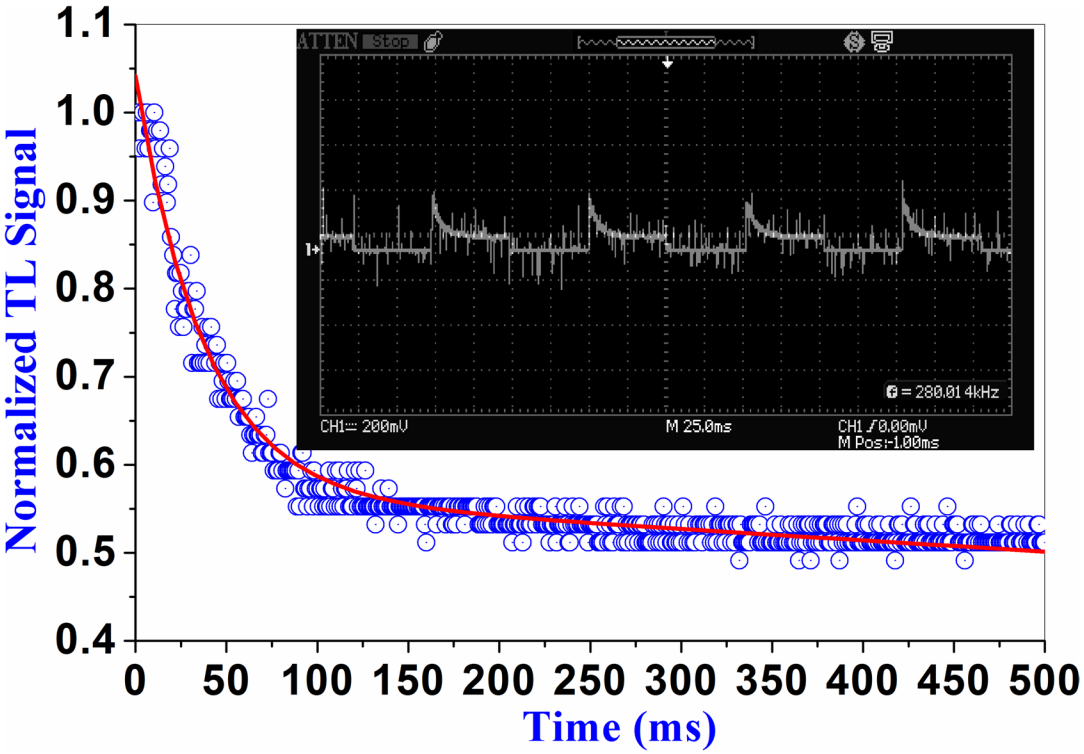

Fig. 13 THLS signal for a Cyanidin-3-O-glucoside chloride dye, the red line corresponds to the data fitting. Inset shows storage oscilloscope THS image

Table 2 Most recently values, oft_c,θ, D_{diff} and dn/dT using the THLS spectrometry method

Sample	t_c	θ(rad)	D_{diff}(cm^2/sec)	dn/dT (K^{-1})	Refs
Er_2O_3 doped SCA	0.8	0.087	5.5×10^{-3}		[81]
Eu_2O_3 doped LSCAS	––	0.062	4.7×10^{-3}	—	[82]
TiO_2: barium titanium borate	1.08	112.8	3×10^{-3}	—-	[83]
Disperse Orange 3	3.8	0.84	8.7×10^{-4}	—	[84]
Yb_2O_3: PbO–Bi_2O_3–Ga_2O_3–BaO	4.47	0.023	2×10^{-3}	1.4×10^{-6}	[85]
Au nanofluid	4.55	1.21	2.52×10^{-3}	—	[86]
CdS-NPs prepared at 30 kGy doses of γ-radiation	0.014	2.013	14.9×10^{-4}	—	[87]
Polymer PPV/SiO_2	201	0.127	3.4×10^{-5}	——	[88]
PbI_2:Sb_2S_3:AS_2S_3	17.5	0.188	1.32×10^{-5}	4.1×10^{-6}	[89]
Nd^{3+} doped Ga_2S_3:La_2:S_3	2.3	0.102	2.7×10^{-3}	7.6×10^{-5}	[90]
Poly-vinyl chloride	5.50	0.079	1.29×10^{-3}	1.14×10^{-4}	[91]
TiO_2 -SiO_2	3.7	0.88	8.8×10^{-4}	––	[92]
tellurite glass	0.57	0.059	2.9×10^{-3}	11.7×10^{-6}	[93]
CoF_2	0.05	0.62	2.8×10^{-3}	16×10^{-6}	[94]
soda lime	5.5	0.079	1.29×10^{-3}	––	[95]
Ga:La:S:O	1.16	0.08	2.6×10^{-3}	4.6×10^{-5}	[96]
poly(2-methoxy) aniline- H_2SO_4	2.21	0.192	1.10×10^{-3}	4.3×10^{-4}	[97]
Azomethine in $CHCl_3$	31.3	0.95	3.92×10^{-5}	-7.17×10^{-5}	[98]
Anthocyanin solution	6.39	0.291	8.9×10^{-4}	3.8×10^{-4}	[98]
CdO–SiO_2	15.13	0.567	7.73×10^{-5}	5.01×10^{-5}	[99]
COGC in DMF	31.3	0.95	6.33×10^{-5}	-8.77×10^{-5}	Present Work

repeat-spin-coating process. Under the wavelength range of 300–900 nm, we determined the amount of absorption that Cyanidin-3-O-glucoside chloride exhibited. At 509 nm, there is a peak in the absorption that occurs regardless of the concentration. This particular wavelength is a component of the conjugated system that is contained inside the chromophore (light-absorbing group) of the Cyanidin-3-O-glucoside chloride dye molecule, and its intensity increases as the concentration of dye sample goes higher. The maximum absorption wavelength of all of the samples remained reasonably consistent around 509 nm, regardless of the quantity of the sample. This paper presents some advancements in the TL and Z-scan techniques for characterising solid-state laser material. The TL technique is used to determine thermal diffusivity, thermal conductivity, and thermooptic coefficient. The TL method is employed to investigate thermal lens signals. the thermal diffusivity is measured to be 6.33×10^{-4} cm^2/sec. The dn/dT and D_{diff} values for the COGC dye were found to be higher than those discovered for other materials, such as CdO-SiO_2 and Azomethine in $CHCl_3$. These values are comparable to those observed for other materials. Based on the findings of all of these experiments, it can be deduced that COGC demonstrates an outstanding nonlinear response and has the potential to be utilised in low-power nonlinear optical systems. Additionally, we demonstrated the application of the Z-scan method to investigate the nonlinear optical properties of COCG solution dye and polymer film. We could directly obtain the nonlinear absorptive and refractive spectra from the normalised transmission using a tunable CW laser source. It has been determined through Z-scan measurements that the COGC:PMMA film displays a nonlinear behaviour that is negative. Based on the measurements, it has been determined that the values of nonlinear absorption coefficients and nonlinear index of refraction are around 10^{-3} cm/W and $10^{-7}$$cm^2$/W, respectively. It is clear that dyes have a significant potential in the production of optical limiters due to the fact that they are environmentally friendly and sustainable.

Competing interest

The authors declare no competing interests.

Authors' Contribution Khitam Alsaedi: Writing – original draft. Abdulameer Imran: software and data curation. Hussain A. Badran: Supervision and Software, Writing – review & editing, Writing – original draft. Riyadh Ch. Abul-Hail: Data curation and analysis of the results, and Khalid I. Ajeel: Compare and analyze figures.

Data Availability No datasets were generated or analysed during the current study.

References

1. Ing RK, Fink M)1998(Time-reversed Lamb waves. IEEE transactions on ultrasonics, ferroelectrics, and frequency control 45(4), 1032–1043. https://doi.org/10.1109/58.710586
2. Shastri BJ, Tait AN, de Ferreira LT, Pernice WH, Bhaskaran H, Wright CD, Prucnal PR (2021) Photonics for artificial intelligence and neuromorphic computing. Nature Photonics. 15(2):102–114
3. Sijo ST, Joe IH (2024) Structural properties and third order nonlinear optical response in Ni0.5 Zn (0.5-x) MnxFe2O4 nanoparticles, Optical Materials. 149: 115009. https://doi.org/10.1016/j.optmat.2024.115009
4. Huang C, Fujisawa S, de Ferreira LTF, Tait AN, Blow EC, Tian Y, Prucnal PR (2012) A silicon photonic–electronic neural network for fibre nonlinearity compensation. Nature Electronics 4(11):837–844
5. Fadhil AT, Hussain AB, Harith AH, Riyadh CA (2023) Azimuthal Angle Scan Distribution, Third Order Response, and Optical Limiting Threshold of the Bismarck Brown Y: PMMA Film. Current Optics and Photonics 7:721–731. https://doi.org/10.3807/COPP.2023.7.6.721
6. Hussain AB, Nadia AHA, Harith AH, Riyadh CAH, Raeed KAF (2023) Synthesis, DSC Properties, Surface Morphology and the Third-Order Behavior Studies of a Conducting Polymer. Polymer Science B 65:858–872. https://doi.org/10.1134/S1560090423600023
7. Abazari R, Yazdani E, Nadafan M, Kirillov AM, Gao J, Slawin AM, Carpenter-Warren CL (2021) Third-order nonlinear optical behavior of an amide-tricarboxylate zinc (II) metal–organic framework with two-fold 3D+ 3D interpenetration. Inorg Chem 60(13):9700–9708
8. Evans OR, Lin W (2002) Crystal engineering of NLO materials based on metal-organic coordination networks. Acc Chem Res 35(7):511–522
9. Ahmed SH, Alaa AA (2016) Effect of Se addition on optical and electrical properties of chalcogenide CdSSe thin films. Superlattices Microstruct 89:153–169. https://doi.org/10.1016/j.spmi.2015.10.044
10. Halasyamani PS, Zhang W (2017) inorganic materials for UV and deep-UV nonlinear-optical applications. Inorg Chem 56(20):12077–12085
11. Ahmed SH (2022) Intensive linear and nonlinear optical studies of thermally evaporated amorphous thin Cu-Ge-Se-Te films. J Non-Cryst Solids 586:121563. https://doi.org/10.1016/j.jnoncrysol.2022.121563
12. Zhang L, Shi XL, Yang YL, Chen ZG (2012) Flexible thermoelectric materials and devices: From materials to applications. Mater Today 46:62–108
13. Saidin S, Jumat MA, Amin NAAM, Al-Hammadi ASS (2021) Organic and inorganic antibacterial approaches in combating bacterial infection for biomedical application. Mater Sci Eng, C 118:111382
14. Mundzir A, Aziz MS, Ganesan K, Fauzan A, Sabah MM, Ibrahim AR, Sulaiman WH (2022) Large third-order optical nonlinear susceptibility in natural dye derived from Clitoria ternatea petal. Optik 256:168752. https://doi.org/10.1016/j.ijleo.2022.168752
15. Fadhil AT, Mohammed TO, Alyaa AJ, Hussain AB, Alaridhee TA (2023) Effect of gamma ray on self- induced diffraction patterns of organic compound Poly(methyl-methacrylate) films. Results in Physics 52:106858. https://doi.org/10.1016/j.rinp.2023.106858
16. Kadem B, Alfahed RKF, Ahmed SA, Hussain AB (2020) Morphological, structural, optical, and photovoltaic cell of copolymer P3HT: ICBA and P3HT:PCBM. Optik 204:164153. https://doi.org/10.1016/j.ijleo.2019.164153

17. Aparna T, Sheenu T, Nampoori VPN (2013) Solvent effect on the third order optical nonlinearity and optical limiting ability of betanin natural dye extracted from red beet root. Optical Materials. 35:2332–2337. https://doi.org/10.1016/j.optmat.2013.06.032
18. Hussain AB, Harith AH (2021) Dielectric constant and conductivity anisotropy measurements of Schiff base liquid crystal. J Phys Conf Ser 1999:012044. https://doi.org/10.1088/1742-6596/1999/1/012044
19. Al-Salihi A, Salim RD, Alfahed, RKF, Hussain AB (2020) Effect of Solar radiation induced and alpha particles on Nonlinear behavior of PM-355 film, IOP Conf. Series: Materials Science and Engineering; 928, 072056. https://doi.org/10.1088/1757-899X/928/7/072056
20. Zongo S, Kerasidou AP, Sone BT, Diallo A, Mthunzi P, Iliopoulos K, Sahraoui B (2015) Nonlinear optical properties of poly (methyl methacrylate) thin films doped with Bixa Orellana dye. Appl Surf Sci 340:72–77
21. Sivakumar V, Vijaeeswarri J, Anna JL, Effective natural dye extraction from different plant, (2011) materials using ultrasound. Ind Crops Prod 33(1):116–122
22. Selvam RM, Athinarayanan G, Nanthini AUR, Singh AR, Kalirajan K, Selvakumar PM (2015) Extraction of natural dyes from Curcuma longa, Trigonella foenum graecum and Nerium oleander, plants, and their application in antimicrobial fabric. Ind Crops Prod 70:84–90
23. Singh LK, Koiry BP (2018) Natural dyes and their effect on efficiency of TiO_2 based DSSCs:a comparative study. Materials Today: Proceedings 5:2112–2122
24. Richhariya G, Kumar A, Tekasakul P, Gupta B (2017) Natural dyes for dye sensitized solar cell: A review. Renew Sustain Energy Rev 69:705–718
25. Bordiga M, Travaglia F, Locatelli M (2019) Valorisation of grape pomace: an approach that is increasingly reaching its maturity-a review. Inter of Food Science Technology 54:933–942
26. Jeyarama S, Geethakrishnan T (2019) Linear and nonlinear optical properties of chlorophyll-a extracted from Andrographis paniculata leaves. Opt Laser Technol 116:31–36. https://doi.org/10.1016/j.optlastec.2019.03.013
27. Jeyarama S (2022) Spectral, third-order nonlinear optical and optical switching behavior of β-carotenoid extracted from phyllanthus niruri. Indian J Phys. 96:1655–1661. https://doi.org/10.1007/s12648-02102122-0
28. Numan N, Jeyaram S, Kaviyarasu K, Neethling P, Sackey J, Kotsedi CL, Akbari M, Morad R, Mthunzi-Kufa P, Sahraou B, Maaza M (2022) On the remarkable nonlinear optical properties of natural tomato lycopene. Sci Rep 12:9078. https://doi.org/10.1038/s41598-022-12196-3
29. Jeyaram S, Geethakrishnan T (2022) Vibrational spectroscopic, linear and nonlinear optical characteristics of *Anthocyanin* extracted from *blueberry*. Results in Optics 1:100010. https://doi.org/10.1016/j.rio.2020.100010
30. Dayang S, Irwanto M, Gomesh N (2016) Nature based dyes from blue pea flower as a potential sensitizer for dssc. Journal of Engineering Research and Education 8:59–66
31. Manikandan KM, Yelilarasi A, Senthamaraikannan P, Saravanakumar SS, Khan A, Asiri AM (2018) The conducting polymer electrolyte based on polypyrrole-polyvinyl alcohol and its application in low- cost quasi-solid-state dye-sensitized solar cells. J Solid State Electrochem 22:3785–3797. https://doi.org/10.1007/s10008-018-4070-4
32. Ahmed SH, Ishu S, Pankaj S (2023) Inference of Sn addition on optical properties of the novel thermally evaporated thin a-Ge15Te50S35-xSnx films and some physical properties of their glasses. Mater Chem Phys 293:126887. https://doi.org/10.1016/j.matchemphys.2022.126887
33. Anthony G, Rui FS, Marvin W (1994) Nonlinear Optics of Organic and Polymers materials. Phys Today 47:51–57. https://doi.org/10.1063/1.881433
34. Rajaa MA, Hussain AB, Riyadh ChA (2024) Electrical, Thermal Lens and Optical Study of Fluorescein Film for Application as Organic Photovoltaic Devices. J Fluoresc 34:549–560. https://doi.org/10.1007/s10895-023-03299-9
35. Alfahed RKF, Dheyaa A, Zahraa Y, Hussain AB, Kareem KM (2023) Preparation and characterization of tin chloride-based polymeric composite for gamma shielding applications. Appl Radiat Isot 196:110774. https://doi.org/10.1016/j.apradiso.2023.110774
36. Ahmed SH, El Radaf IM (2023) Effect of fluorine doping on the structural, optical, and electrical properties of spray deposited Sb_2O_3 thin films. Mater Sci Semicond Process 160:107405. https://doi.org/10.1016/j.mssp.2023.107405
37. Al-Fahed RKF, Alaa AR, Munaf SM, Hussain AB (2021) Chemical Polymerization Method to Synthesize Polyaniline as a Novel Anode Catalyst in Microbial Fuel Cell. Polym Sci B 63:773–780. https://doi.org/10.1134/S1560090421060026
38. Hanan AA, Alfahed RKF, Imran A, Hussain AB, Hussain SS, Alsalihi AA (2019) Preparation and optoelectronic studies of the organic compound [2- (2,3- dimethyl phenylamino)- N-Phenyl benzamide] doped PMMA. J Mater Sci Mater Electron 30:10284–10292. https://doi.org/10.1007/s10854-019-01365-2
39. Hussain AB, Taha AY, Abdulkader AF, Emshary CA (2012) preparation and study of the electrical and optical properties of a new azo dye (4-acetaminophenol-[2-(4-azo)]- 4- amin sulfone) J Ovonic Res. 8:161–70.
40. Hussain AB (2012) Study on Optical Constants and Refractive Index Dispersion of Neutral red Doped Polymer Film. Am J Appl Sci 9:250–253. https://doi.org/10.3844/ajassp.2012.250.253
41. Al-Salihi A, Salim RD, Alfahed RKF, Hussain AB (2020) Effect of Solar radiation induced and alpha particles on Nonlinear behavior of PM-355 film. IOP Conf Series Mater Sci Eng 928:072056. https://doi.org/10.1088/1757-899X/928/7/072056
42. Sheik-Bahae M, Said AA, Wei T, Hagan DJ, Van Stryland EW (1990) Sensitive measurement of optical nonlinearities using a single beam. IEEE J Quant Electron QE 26:760–769
43. Al-Saymari FA, Hussain AB, Alaa YA, Chassib AE (2013) Time dependent diffraction ring patterns in bromothymol blue dye doped PMMA film under irradiation with continuous wave green laser light. Indian J Phys 87:1153–1156. https://doi.org/10.1007/s12648-013-0334-0
44. RKF Alfahed, I Abdulameer, MS Majeed, Hussain AB (2020) Photoluminescence characterizations and nonlinear optical of PM-355 nuclear track detector film by alpha-particles and laser irradiation. Phys Scr. 95:075709 (8 pp) https://doi.org/10.1088/1402-4896/ab7e33
45. Hussain AB, Al-Fregi AA, Alfahed RF, Al-Asadi AS (2017) Study of thermal lens technique and third-order nonlinear susceptibility of PMMA base containing 5′, 5″- dibromo-o-cresolsulfo-phthalein. J Mater Sci Mater Electron 28:17288–17296. https://doi.org/10.1007/s10854-017-7661-4
46. Alfahed RKF, Al-Asadi AS, Al-Mudhaffer M, Hussain AB (2021) Synthesis, morphological and optical characterizations of the poly (O-toluidine) LiCl networks thin film. Opt Laser Technol 133:106524. https://doi.org/10.1016/j.optlastec.2020.106524
47. Hussain AB, Hussain FH, Ajeel KI (2016) Nonlinear characterization of conducting polymer and electrical study for application as solar cells and its antibacterial activity. Optik 127:5301. https://doi.org/10.1016/j.ijleo.2016.03.030
48. Hussain AB, Al-Maliki A, Alfahed RKF, Saeed BA, Al-Ahmad AY, Al- Saymari FA, Elias RS (2018) Synthesis, surface profile, nonlinear reflective index and photophysical properties of curcumin compound. J Mater Sci Mater Electron 29:10890–10903. https://doi.org/10.1007/s10854-018-9167-0

49. Alfahed RF, Al-Asadi AS, Hussain AB, Khalid IA (2019) Structural, morphological, and Z-scan technique for a temperature-controllable chemical reaction synthesis of zinc sulfide nanoparticles. Appl Phys B 125:48. https://doi.org/10.1007/s00340-019-7154-7
50. Hussain AB, Abul-Hail RC, Mohammed TO (2020) Study on effect of gamma radiation on some linear and nonlinear properties of Pyronine Y. AIP Conf Proc 2290:35–50. https://doi.org/10.1063/5.0027452
51. AL-AdelHussain KAAB (2012) Nonlinear optical properties and diffraction ring patterns of benzo congo red. Eur J Appl Eng Sci Res 1:66–72
52. Abdulah AH, Musa AA, Alfahed RKF, Hussain AB (2020) Diffracting samples Nonlinear:optical properties and morphology for (2- hydroxyphenyl) [2-(2- methoxybenzylideneamino)-5-methyl phenyl] telluride film. AIP Conf Proc 2290:050049. https://doi.org/10.1063/5.0027845
53. Hussain AB (2012) Investigation of the nonlinear optical response of 3-(dimethylamino)- 7- aminopheno thiazin- 5-ium chloride dye. IOSR J Appl Phys.1:33–7.
54. Hussain AB, Hanan AA, Alfahed RKF, Khalid IA (2021) Second-order hyperpolarizability and nonlinear optical properties of novel organic compound-doped poly (O-methoxyaniline) polymer film. J Mater Sci Mater Electron 32:14623–41629. https://doi.org/10.1007/s10854-021-06021-2
55. Harith AH, Nadia AHA, Hussain AB, Alfahed RK, Khalid IA (2024) The influence of temperature on structural and third order nonlinear properties of cadmium sulfide nanoparticle films prepared by chemical reaction method. Mater Res Bull 170:112554–112367. https://doi.org/10.1016/j.materresbull.2023.112554
56. Hussain AB, Alyaa AJ (2017) Measurements of third-order susceptibility of 3-[[(4-methyl-1-piperazinyl imino]-methyl]-rifamycin vs using z-scan technique. Int Res J Nat Appl Sci 4:29–38
57. Bouchouit K, Derkowska B, Migalska-Zalas A, Abed S, Benalicherif N, Sahraoui B (2010) Nonlinear optical properties of selected natural pigments extracted from spinach: carotenoids. Dyes Pigm 86:161–165. https://doi.org/10.1016/j.dyepig.2009.12.013
58. Sudha N, Surendran R, Jeyaram S (2022) Synthesis, Spectral, Solvent Dependent Linear and Nonlinear Optical Characteristics of (E)-N-(3-(3-(4(dimethylamino)phenyl)acryloyl) phenyl) quinolone-2-carboxamide. J Fluoresc 32:1471–1480. https://doi.org/10.1007/s10895-022-02959-6
59. Prakash J, Jeyaram S (2022) Synthesis, Characterization, Morphological, Linear and Nonlinear Optical Properties of Silicon Carbide Doped PVA Nanocomposites. SILICON 14:11163–11170. https://doi.org/10.1007/s12633-022-01852-y
60. Sudha N, Surendran R, Jeyaram S (2024) Vibrational spectroscopic, structural, linear and third-order nonlinear optical properties of isoniazid-vanillin hybrid. Indian J Phys 98:1453–1462. https://doi.org/10.1007/s12648-023-02869-8
61. Sudha N, Surendran R, Jeyaram S (2023) Low power Z–scan studies of Schiff base (E)-N'-(4-(dimethylamino) benzylidene) isonicotinohydrazide for nonlinear optical applications. Indian J Phys 97:4399–4408. https://doi.org/10.1007/s12648-023-02764-2
62. Dini D, Calvete MJ, Hanack M (2016) Nonlinear optical materials for the smart filtering of optical radiation. Chemical reviews. 116:13043–13233
63. Zhou GJ, Wong WY (2011) Organometallic acetylides of Pt II, Au I and Hg II as new generation optical power limiting materials. Chem Soc Rev 40:2541–2566
64. Shanyi G, Shouchun Y, Hongyao X, Weiju Z, Yachen G, Yinlin S (2007) Synthesis and properties of long conjugated organic optical limiting materials with different π-electron conjugation bridge structure. Dyes Pigm 73:285–291. https://doi.org/10.1016/j.dyepig.2005.12.005
65. Mohammed TO, Abul-Hail RC, Hussain AB (2020) Gamma irradiation effect on the nonlinear refractive index and optical limiting behavior of pyronine Y dye solution. Journal of Basrah Researches (Sciences) 46:49–56
66. Abdulameer I, Sattar JB, Abdalrahman A, Hussain AB (2020) Gamma irradiation impact on the morphology and thermal blooming of sodalime glass. AIP Conf Proc 2290:050038. https://doi.org/10.1063/5.0031473
67. Franko M, Tran CD (1991) Thermal Lens Technique for Sensitive Kinetic Determinations of Fast Chemical Reactions. Part I. Theory. Rev Sci Instrum 62:2430–2437
68. Shen J, Lowe RD, Snook RD (1992) A model for cw laser induced mode mismatched dual-beam thermal lens spectrometry. Chem Phys 165:385–396
69. Lima SM, Souza AKR, Langaro AP, Silva JR, Costa FB, Moraes JCS, Figueiredo MS, Santos FA, Baesso ML, Nunes LAO, Andrade LHC (2016) Fluorescence quantum yield of Yb3-doped tellurite glasses determined by thermal lens spectroscopy. Opt Mater 63:19–25. https://doi.org/10.1016/j.optmat.2016.08.042
70. Hussain AB (2014) Thermal lens and all optical switching of new organometallic compound doped polyacrylamide gel. Results Phys 4:69–72. https://doi.org/10.1016/j.rinp.2014.05.004
71. Santhi AJ, Misha H, Mathew S, Gaurav S, Soumya HVM, Radhakrishnan P, Nampoori VPN (2010) Thermal diffusivity of rhodamine 6G incorporated in silver nanofluid measured using mode matched thermal lens technique. Optics Communications 283:313–317. https://doi.org/10.1016/j.optcom.2009.10.016
72. Alfahed RKF, Abdulameer I, Hussain AB, Abdalrahman A (2020) Synthesis, optical limiting behavior, thermal blooming and nonlinear studies of dye doped polymer films. J Mater Sci Mater Electron 31:13862–13873. https://doi.org/10.1007/s10854-020-03946-y
73. Hussain AB, Al-Ahmad AY, Al-Mudhaffer MF, Chassib AE (2014) Nonlinear optical responses and limiting behavior of sulfadiazine-chromotropic acid azo dye. Opt Quant Electron 46:1859–1867. https://doi.org/10.1007/s11082-014-0051-8
74. Jacinto C, Messias DN, Andrade AA, Lima SM, Baesso ML, Catunda T (2006) Thermal lens and Z- scan measurements: Thermal and optical properties of laser glasses-A review. Journal of Non-Crystalline Solid 352:3582–3597
75. Ventura M, Simionatto E, Andrade LHC, Simionatto EL, Riva D, Lima SM (2013) The use of thermal lens spectroscopy to assess oil–biodiesel blends. Fuel. 103:506–511. https://doi.org/10.1016/j.fuel.2012.08.027
76. Sampaio JA, Catunda T, Gama S, Baesso ML (2001) Thermo-optical properties of OH-free erbium doped low silica calcium aluminosilicate glasses measured by thermal lens. Journal of Non-Crystalline Solid 284:210–2216
77. Hussain AB, Khalid IA, Lazim HG (2016) Effect of nano particle sizes on the third-order optical nonlinearities and nanostructure of copolymer P3HT: PCBM thin film for organic photovoltaics. Mater Res Bull 76:422–430. https://doi.org/10.1016/j.materresbull.2016.01.005
78. Lazim HG, Ajeel KI, Badran HA (2015) The photovoltaic efficiency of the fabrication of copolymer P3HT: PCBM on different thickness nano-anatase titania as solar cell. Spectrochim Acta A Mol Biomol Spectrosc 145:598–603. https://doi.org/10.1016/j.saa.2015.02.096
79. Alfahed RKF, Hussain AB, Abu Talib YA, Noor AS (2021) Investigation of third order nonlinearity of Ethidium bromide doped deoxyribonucleic acid (DNA). J Phys Conf Ser 1963:012136. https://doi.org/10.1088/1742-6596/1963/1/012136
80. Fahimeh A, Mahsa F (2024) Improvement in optical nonlinearity of spiral square Mn-based nanostructures with increasing the number of square sides. Optik 311:171919. https://doi.org/10.1016/j.ijleo.2024.171919

81. Andrade AA, Coutinho MF, de Castro MPP, Vargas H, Rohling JH, Novatski A, Astrath NGC, Pereira JRD, Bento AC, Baesso ML, Oliveira SL, Nunes LAO (2006) Luminescence quantum efficiency investigation of low silica calcium aluminosilicate glasses doped with Eu_2O_3 by thermal lens spectrometry. Journal of Non-Crystalline Solids 352:3624–3627. https://doi.org/10.1016/j.jnoncrysol.2006.03.092
82. Jacinto C, Feitosa CAC, Mastelaro VR, Catunda T (2006) Thermal properties of barium titanium borate glasses measured by thermal lens technique. J Non-Cryst Solids 352:3577–3581. https://doi.org/10.1016/j.jnoncrysol.2006.03.089
83. Harith AH, Nadia AHAA, Hussain AB, Raeed KA, Khalid IA (2023) Effects of temperature on structural and linear/nonlinear optical properties of CdS nanoparticles film deposited by chemical reaction method. Opt Quant Electron 55:555. https://doi.org/10.1007/s11082-023-04835-4
84. Kassab LRP, Del Cacho VD, Bell MJV, Messias DN, De Oliveira SL, Catunda T (2006) Thermal lens study of PbO–Bi_2O_3–Ga_2O_3–BaO glasses doped with Yb^{3+}. J Non-Cryst Solids 352:3647–3652. https://doi.org/10.1016/j.jnoncrysol.2006.03.097
85. Shahriari E, Yunus WMM, Zamiri R (2013) The effect of nanoparticle size on thermal diffusivity of gold nano-fluid measured using thermal lens technique. J Europ Opt Soc Rap Public 8:13026–13030. https://doi.org/10.2971/jeos.2013.13026
86. Azmi Z, Reza Z, Parisa V, Elias S, Husin MS (2011) Thermal Diffusivity Measurement of Cadmium Sulphide Nanoparticles Prepared by γ-Radiation Technique. World Academy of Science, Engineering and Technology 79:92–94
87. Pilla V, Andrade AA, Lima SM, Catunda T, Donatti DA, Vollet DR, Ruiz AI (2003) Spectroscopic and thermal characterization in poly(*p*-phenylene vinylene)/sol–gel silica sample Opt. Mater 24:483–489. https://doi.org/10.1016/S0925-3467(03)00032-6
88. Lima SM, Andrade AA, Catunda T, Lebullenger R, Smektala F, Jestin Y, Baesso ML (2001) Thermal and optical properties of chalcohalide glass. J Non-Cryst Solids 284:203–209
89. Lima SM, Sampaio JA, Catunda T, Ca De, Argo, (2001) Nunes LAO, Baesso ML, Hewak DW. Spectroscopy, thermal and optical properties of Nd^{3+} doped Chalcogenide glasses. J Non-Cryst Solids 284:274–281
90. Rohling JH, Caldeira AMF, Pereira JRD, Medina AN, Bento AC, Baesso ML, Miranda LCM (2011) Thermal lens scanning of the glass transition in polymers. J Appl Phys 89:2220–2226. https://doi.org/10.1063/1.1333737
91. Enlin C, Linhong H, Shanming L, Min C, Shuaiyi Z, Xinxing L, Yin H (2025) Nonlinear optical response and application of indirect narrow-bandgap SbTe nanosheets. Opt Laser Technol 180:111563. https://doi.org/10.1016/j.optlastec.2024.111563
92. Pilla V, Chillcce EF, Neves AAR, Munin E, Catunda T, Cesar CL, Barbosa LC (2007) Thermal lens study of thermo-optical properties of tellurite glasses. J Mater Sci 42:2304–2308. https://doi.org/10.1007/s10853-006-0180-y
93. Lima SM, Sampaio JA, Catunda T, Bento AC, Miranda LCM (2000) Mode-mismatched thermal lens spectrometry for thermo-optical properties measurement in optical glasses: a review. Journal of Non-Crystalline Solid 373:215. https://doi.org/10.1016/S0022-3093(00)00169-1
94. Rohling JH, Medina AN, Pereira JRD, Rubira AF, Bento AC, Miranda LCM, Baesso ML (2001) Thermal lens versus DSC measurements for glass transition analysis of polymer. Anal Sci 17:s103–s105
95. Lima SM, Steimacher A, Medina AN, Baesso ML, Petrovich MN, Rutt HN, Hewak DW (2004) Thermo optical properties measurements in chalcogenide glasses using thermal relaxation and thermal lens methods. J Non-Cryst Solids 348:108–112. https://doi.org/10.1016/j.jnoncrysol.2004.08.134
96. Andrade AA, Castro MPP, Rocha AM, Vargas H, Bastos NMS, Giacomini RA, Miranda PCML, Jacinto C, Catunda T (2007) Evaluation of thermo-optical properties of poly (2-methoxyaniline) solutions. Chem Phys Lett 442:400–404. https://doi.org/10.1016/j.cplett.2007.06.021
97. Hussain AB (2015) Thermal properties of a new dye compound measured by thermal lens effect and Z-scan Technique. Appl Phys B 119:319–326. https://doi.org/10.1007/s00340-015-6068-2
98. Vanessa M, Sthanley RdL, Jaqueline OBT, Andrea A, Djalmir NM, Acácio AA, Noelio OD, Sérgio CZ, Viviane P (2016) Preliminary Spectroscopic and Thermo-optical Characterization of Anthocyanin Unpurified Crude Extracted from Tradescantia Pallida Purpurea. Dyes Pigm 135:57–63. https://doi.org/10.1016/j.dyepig.2016.06.020
99. Badran HA, AL Aladil KA, LazimAl-Ahmad HGAY (2016) Thermal blooming and photolumines-cence characterizations of sol–gel CdO–SiO_2 with different nanocomposite. J Mater Sci Mater Electron 27:2212–2220. https://doi.org/10.1007/s10854-015-4013-0